First publ. in: Physical Review Letters 102 (2009), 238301

Ultrafast Quenching of Binary Colloidal Suspensions in an External Magnetic Field

Lahcen Assoud,[1] Florian Ebert,[2] Peter Keim,[2] René Messina,[1] Georg Maret,[2] and Hartmut Löwen[1]

[1]*Institut für Theoretische Physik II: Weiche Materie, Heinrich-Heine-Universität Düsseldorf, Universitätsstraße 1, D-40225 Düsseldorf, Germany*

[2]*Fachbereich für Physik, Universität Konstanz, D-78457 Konstanz, Germany*

An ultrafast quench is applied to binary mixtures of superparamagnetic colloidal particles confined at a two-dimensional water-air interface by a sudden increase of an external magnetic field. This quench realizes a virtually instantaneous cooling which is impossible in molecular systems. Using real-space experiments, the relaxation behavior after the quench is explored. Local crystallites with triangular and square symmetry are formed on different time scales, and the correlation peak amplitude of the small particles evolves nonmonotonically in time in agreement with Brownian dynamics computer simulations.

PACS numbers: 82.70.Dd, 61.20.Ja

Temperature quenching belongs to the key processing techniques to produce amorphous and crystalline solids which are considerably different from their thermodynamically stable counterparts. Possible applications can be found in metallurgy, ceramics, and semiconductor doping. For example, quenching is used to construct ceramic material with a high mechanical stability [1], to design resistance devices for integrated circuits [2], and to improve the optoelectronic properties of semiconductors [3].

Temperature quenching techniques are most efficient if they are performed suddenly, i.e., if the system temperature changes on a time scale that is much shorter than a time upon which a typical particle motion is performed. While this can be realized in computer simulations, see, e.g., [4–6], it is practically impossible to be achieved for molecular systems where the quench is performed by a coupling to an external heat bath. There, it takes some time until the prescribed temperature is realized in the sample. However, as we shall show in this Letter, an ultrafast quenching is possible for colloidal particles which move much slower and are highly susceptible to external fields.

If a suspension of superparamagnetic particles is used, an external magnetic field induces magnetic dipoles in the particles which gives rise to dipolar interactions between them [7]. In equilibrium, temperature and magnetic field strength determine the dimensionless coupling strength between the particles such that temperature is strictly equivalent to the inverse square of the magnetic field strength [8,9]. Therefore a sudden increase of the external magnetic field corresponds to an ultrafast quench towards lower temperature. It is important to note that the increase of the external magnetic field occurs on a time scale of a few ms much smaller than a couple of seconds typically needed by a colloidal particle to diffuse over its own size. Thereby—unlike molecular systems—colloidal systems can be exposed to ultrafast temperature quenches.

In this Letter, we exploit this idea of quasi-instantaneous quenching for a binary suspension of two-dimensional superparamagnetic colloidal particles confined to a planar water-air interface. At high temperatures—or equivalently at low external magnetic field strengths—the system is weakly correlated. After an abrupt increase of the external magnetic field, the response of the system and the early stage relaxation towards its new state is monitored by real-space imaging. For the prescribed composition of the mixture, the equilibrium state is a crystalline lattice with alternating stripes of pure triangles of the majority component and mixed squares [10]. This complicated stable crystal is not reached on the time scale explored, but the system reveals structural heterogeneities corresponding to local metastable patches of crystalline order. These crystalline zones are forming on different time scales which also gives rise to nonmonotonic behavior in time for structural correlation peaks of the small particles. The real-space experiments are in agreement with our Brownian dynamics computer simulations. Our results can be used to steer the microstructure of composite materials upon quenching and reveal the interplay between vitrification and crystal nucleation [11].

The experimental system consists of a suspension of two kinds of spherical superparamagnetic colloidal particles denoted by A and B. Those particles are characterized by different diameters ($d_A = 4.5\ \mu$m, $d_B = 2.8\ \mu$m) and magnetic susceptibilities ($\chi_A = 6.2 \times 10^{-11}\ \mathrm{A\,m^2/T}$, $\chi_B = 6.6 \times 10^{-12}\ \mathrm{A\,m^2/T}$). The relative composition $X = N_B/(N_A + N_B)$ of B particles is fixed at 40%. Because of their high mass density, the particles are confined by gravity to a flat water-air interface formed by a pending water drop. The droplet is suspended by surface tension in a top sealed cylindrical hole (6 mm diameter, 1 mm depth) on a glass plate. The system can be considered as ideally two dimensional since the thermally activated ''out of plane'' motion of the particles is of the order of a few tens of nanometer. A coil produces a magnetic field $\vec{H}$ perpendicular to the water-air interface inducing a magnetic moment ($\vec{m}_i = \chi_i \vec{H}$ with $i = A, B$) in each par-

ticle which leads to a repulsive dipole-dipole pair interaction of the form

$$u_{ij}(r) = \frac{\mu_0}{4\pi}\chi_i\chi_j H^2/r^3 \qquad (i, j = A, B). \tag{1}$$

For this inverse power potential, at fixed composition X and susceptibility ratio χ_B/χ_A, all static quantities depend solely [12] on a dimensionless interaction strength (or coupling constant)

$$\Gamma = \frac{\mu_0}{4\pi}\frac{\chi_A^2 H^2}{k_B T a^3}, \tag{2}$$

where $k_B T$ is the thermal energy at room temperature and $a = 1/\sqrt{\rho_A}$ the average interparticle separation between A particles. The partial A particle density is set to $\rho_A = 1.97 \times 10^{-3}\ \mu\text{m}^{-2}$ so that $a \simeq 22.5\ \mu$m. The pair interaction is directly controlled over a wide range via the magnetic field. Making use of video microscopy, trajectories of all particles in the field of view can be recorded over several days providing the whole phase space information. The quench was realized upon suddenly rising the coupling Γ from 1 to 71 at time $t = 0$ by increasing the magnetic field. The time scale of the quench is only limited by the electronics of power supply and was measured to be 5 ms. This is much faster than the typical Brownian time $\tau = d_A^2/(4D_A)$ (≈ 50 s) needed for an A particle to diffuse over its own radius with $D_A = 0.11\ \mu\text{m}^2/\text{s}$ being the short-time diffusion constant for A particles. Hence the quench can be considered to be ultrafast [13]. In an unquenched system, clear deviations from purely diffusive behavior appear already at about $\Gamma \approx 30$ [7]. For $\Gamma = 71$ a well-pronounced plateau between $t/\tau = 2$ and $t/\tau = 200$ is observed in the mean-square displacement with an inflection point at $t/\tau = 40$ [7]. Additional computer simulations reveal that the equilibrium crystallization from a liquid occurs again at $\Gamma = 30$. Hence the ultrafast quench leads deeply into the supercooled state.

In parallel, we perform nonequilibrium Brownian dynamics (BD) computer simulations [14] of our experimental system described above neglecting hydrodynamic interactions as the area fraction is small, on the 1% level. We employ pointlike dipoles that interact following Eq. (1) with $\chi_B/\chi_A = 10\%$ and $X = 40\%$ in accordance to the experimental parameters. Knowing that the diffusion constant scales with the inverse of the radius of a particle, D_B was chosen such that $D_B/D_A = d_A/d_B$. $N_A = 400$ A particles and $N_B = 267$ B particles were placed in a square box with periodic boundary conditions applied in the two directions. A finite time step $\delta t = 6 \times 10^{-4}\tau$ was used. The early stage of the system response to the ultrafast quench has been observed both in real-space experiments and BD computer simulations and was characterized by various time-dependent correlations. Our first aim is to identify the dynamical formation of local crystallites after the quench and detect building blocks of the underlying equilibrium crystal. The latter consists of alternating stripes of pure A triangles and intersecting squares of A and B particles [10]. Therefore we have used criteria to define A particles which have a pure triangular surrounding of other A particles, i.e., which are close to a cutout of a pure triangular A crystal, and, likewise, we have identified A and B particles which form locally an equimolar square lattice $S(AB)$ [15]. The corresponding two structure elements are shown as insets in Fig. 1. In detail, we associate a triangular surrounding to an A particle if the following two criteria are fulfilled simultaneously [9]. (1) The sixfold bond order parameter $p_6 = \sqrt{\Psi_6^* \Psi_6}$ [where $\Psi_6 = \frac{1}{6} \times \sum_{NN}^{6} \exp(i6\theta_{NN})$ with θ_{NN} denoting the angles of the six nearest neighbor bonds relative to a fixed reference] is larger than 0.94. (2) The relative bond length deviation $b_6 = \frac{1}{6}\sum_{NN}^{6} \frac{|l_{NN} - \bar{l}|}{\bar{l}}$ where $\bar{l}$ is the average length of the six bond lengths l_{NN} is smaller than 0.04. This double condition selects local configurations close to those of a perfect triangular lattice where p_6 is unity and b_6 vanishes. Likewise we define a square surrounding around a B

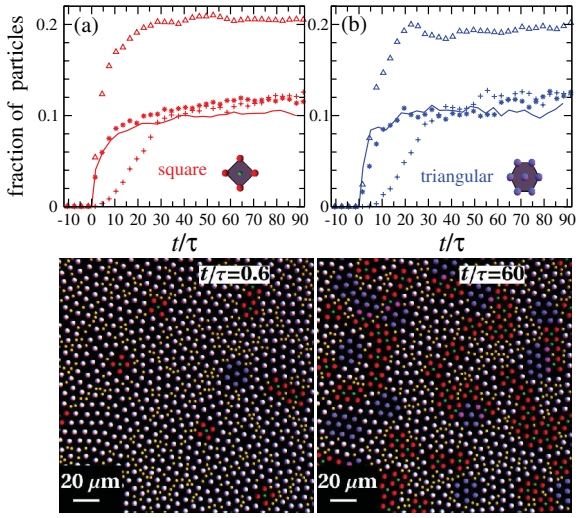

FIG. 1 (color). (a) Fraction of B particles belonging to a crystalline square surrounding (see inset) and (b) fraction of A particles belonging to a crystalline triangular surrounding (see inset) versus reduced time t/τ for an ultrafast quench from $\Gamma = 1$ to $\Gamma = 71$. The lines are experimental data while the symbols (*) are data from BD simulations. Two experimental snapshots for a time $t/\tau = 0.6$ just after the quench (left configuration) and a later time $t/\tau = 60$ (right configuration) are shown. Big particles are shown in blue if they belong to a triangular surrounding and in red if they belong to a square surrounding. All other big particles are shown in white. Few big particles belonging to both triangular and square surroundings are shown in pink. The small particles are shown in green if they belong to a square center of big particles, otherwise they appear in yellow. Also included are simulation data for an instantaneous "steepest descent" quench from $\Gamma = 1$ to $\Gamma = \infty$ ($\triangle$) and for a linear increase of Γ from $\Gamma = 1$ to $\Gamma = 71$ on a time scale of 30τ (+).

particle by the following criteria. (1) The fourfold bond order parameter $p_4 = \sqrt{\Psi_4^* \Psi_4}$ [where $\Psi_4 = \frac{1}{4} \times \sum_{NN}^{4} \exp(i4\theta_{NN})$ with θ_{NN} denoting the bond angles of the four nearest neighbor AB bonds] is larger than 0.92. (2) The corresponding relative AB bond length deviation b_4 is smaller than 0.05.

Experimental snapshots before and after the instantaneous quench are shown in Fig. 1 with color-coded particles indicating the locations of A and B particles which belong to local triangular and square clusters. If an A particle has a triangular surrounding, all seven A particles including the central one with its full surrounding are shown in blue. Conversely, if a B particle has a square surrounding, it is colored in green and its four A neighbors are colored in red. All particles which belong both to the blue and the red class are shown in pink. From the snapshots of Fig. 1, it is evident that the crystalline clusters form locally and grow as a function of time. Preferentially triangular structures form in an area depleted from B particles while square structures nucleate around "seeds" which possess a structure close to an underlying square. The resulting crystalline patches are then fluctuating with a lifetime of about 30τ. The fraction of A particles with a triangular surrounding and of B particles with a square surrounding are shown as a function of time in Figs. 1(a) and 1(b), respectively. On the time scale considered in this plot one finds an increase from almost zero before the quench to 12% for the triangular A particles and the square B particles. The time scales upon which triangular and square structures are formed are different by a factor of about 2. The triangular structure is forming more rapidly than the square one. This follows from the fact that an AB square structure requires more fine-tuning of structural correlations of both species than a triangular one which can directly emerge in regions depleted from small particles. The number of pink A particles which belong to both triangular and square surroundings is growing on a time scale slightly longer than that for the square structure to a fraction of only 1%–2% far away from the equilibrium structure where the fraction of pink particles is 2/3.

After a relaxation time of $t = 10\tau$, we have further calculated the mean-square displacements for particles which are crystalline (i.e., colored in blue, red, green) and noncrystalline particles during a time of 60τ; see Fig. 1. In both experiment and simulation, for both particles species the mean-square displacement of the uncolored particles is twice as large as that of the colored ones. This gives clear evidence for a correlation between local slow dynamics and local crystallinity.

By simulation we have finally explored a different depth and rate of the quench (see Fig. 1). While a "steepest descent" quench leads to a faster growth of crystalline patches and to an almost doubled crystalline fraction of particles, a linear increase of Γ within a time window of 30τ delays their formation accordingly.

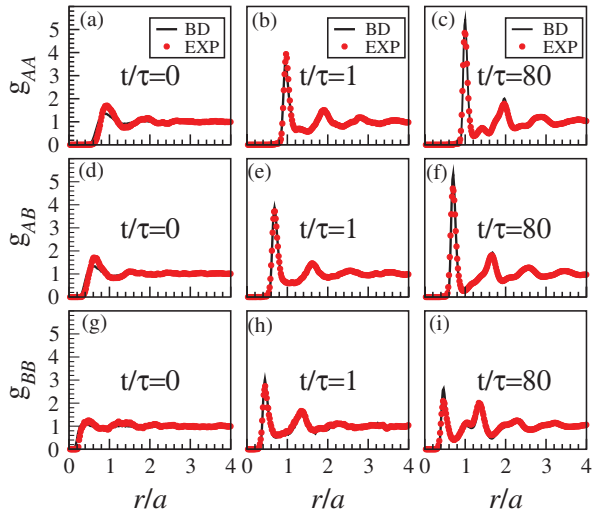

FIG. 2 (color). Partial pair distribution functions $g_{AA}(r)$, $g_{AB}(r)$, and $g_{BB}(r)$ of A and B particles versus reduced distance r/a at three different reduced times (a),(d),(g) $t/\tau = 0$, (b),(e), (h) $t/\tau = 1$, (c),(f),(i) $t/\tau = 80$. BD results (solid lines) are compared to experimental data (symbols).

Next we show the time evolution of the partial pair distribution functions $g_{AA}(r)$, $g_{AB}(r)$, and $g_{BB}(r)$ for three times $t/\tau = 0, 1, 80$ in Fig. 2. While the correlations in the starting configurations before the quench are weak, they are quickly increasing as a function of time towards a strongly correlated glass. An averaged square order can be extracted from the growth of an intermediate peak in $g_{AA}(r)$ at $r = \sqrt{2}a$. This peak grows much slower than the first peak amplitude. The growth of the first peak amplitude in $g_{AA}(r)$ and $g_{AB}(r)$ are monotonic in time, whereas there is a nonmonotonicity in that of $g_{BB}(r)$. This is clearly visible in Fig. 3 where the dynamical evolution of the amplitudes of all three partial pair distribution functions is shown. Within the statistical accuracy, the peaks of $g_{AA}(r)$ and $g_{AB}(r)$ grow on the same time scale in a monotonic way, while the peak of $g_{BB}(r)$ overshoots its final equilibrium limit, both in experiment and simulation [16]. We explain this striking effect by a two-stage relaxa-

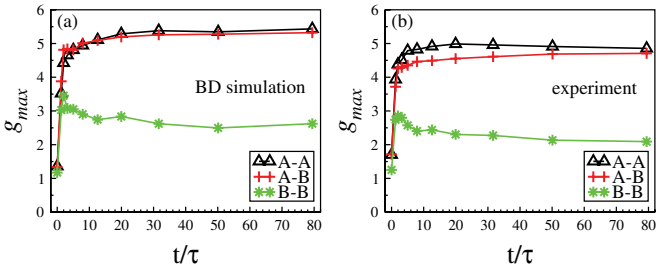

FIG. 3 (color). Amplitude $g_{\max}$ of the first correlation peak in the partial pair distribution function $g_{AA}(r)$ (triangles), $g_{AB}(r)$ (crosses), $g_{BB}(r)$ (stars) as a function of reduced time t/τ. Note the nonmonotonicity in the amplitude of $g_{BB}(r)$. (a) Brownian dynamics data and (b) experiments.

tion process of the small particles which are first excluded from the triangular crystallites regions of the big ones. Concomitantly they show a strong correlation since they are compressed until the total system relaxes back to a state where the small particles optimize their correlations in the network dictated by the big ones.

The energetic optimization to the final state is shown in Fig. 4. There is a huge jump in the potential energy per particle immediately after the quench which then relaxes quickly towards a transient state. Then, on a second time scale, we find a slower relaxation process accompanied by a structural ordering as can be seen in the corresponding experimental snapshots right before and after the instantaneous quench (see inset of Fig. 4). The discrepancy between simulation and experiment for $t < 0$ may be attributed to additional interparticle forces as originating from Earth's magnetic field or other magnetic stray fields. For $t > 0$, on the other hand, there is agreement on the level of uncertainties of the particle susceptibilities.

In conclusion, we have realized an ultrafast quench in two-dimensional colloidal mixtures from a weakly interacting to a strongly interacting situation by a sudden increase of an external magnetic field which controls the interparticle repulsion. The system spontaneously relaxes by exhibiting structural inhomogeneities which reflect the underlying stable crystal and correlate with slower regions in the dynamics. The experimental data are in good agreement with Brownian dynamics computer simulations.

Our real-space characterization allows us to identify the pathways of relaxation into a quenched glassy phase. As the quench is ultrafast, the dynamical pathways are not blurred by an additional time scale from the quench history. The buildup and the fluctuations of local crystallites after the quench can be directly followed. Therefore our analysis can help in a more fundamental way to understand the interplay between vitrification and crystallization [11]. In fact, the structural heterogeneities detected here give a considerable weight to concomitant dynamical heterogeneities [17,18] and could therefore represent a relevant contribution to the dynamical heterogeneity of glasses [19,20]. However, one should bear in mind that the system considered here is strongly driven and there is no aging in the glass. Finally, our results may also be useful to identify pathways of defect annealing in the crystalline phase [21–23].

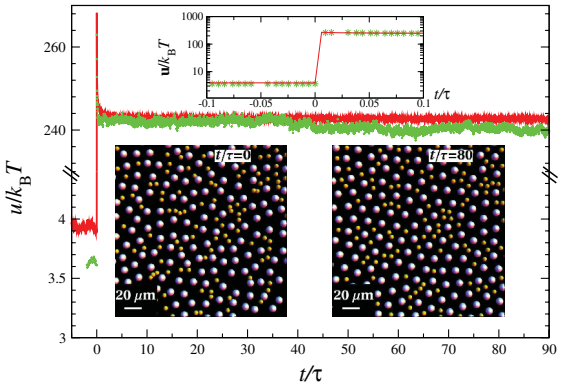

FIG. 4 (color). Time evolution of the potential energy u per particle in units of k_BT versus reduced time t/τ. Brownian dynamics simulation data are shown in red, experimental data in green. For a better comparison the jump after the quench is truncated (see the cut in the y axis). The inset is an expanded view. Corresponding experimental snapshots are shown before the quench at $t/\tau = 0^-$ on the left-hand side and after the quench at $t/\tau = 80$ on the right-hand side. Big particles are shown in white while small particles are presented as yellow spheres.

We thank Patrick Dillmann for helpful discussions. This work was supported by the DFG (projects C2 and C3 of SFB TR6 and SPP 1296).

[1] J. H. She, T. Ohji, and Z. Y. Deng, J. Am. Ceram. Soc. **85**, 2125 (2002).
[2] Q. Shao *et al.*, Appl. Phys. Lett. **92**, 202108 (2008).
[3] J. M. Zavada *et al.*, J. Alloys Compd. **300**, 207 (2000).
[4] R. Yamamoto and K. Nakanishi, Phys. Rev. B **49**, 14 958 (1994).
[5] L. N. Yakub, Low Temp. Phys. **29**, 780 (2003).
[6] J. C. Arce, C. Schaadt, and H. J. Bart, Chem. Eng. Technol. **29**, 487 (2006).
[7] H. König *et al.*, Eur. Phys. J. E **18**, 287 (2005).
[8] N. Hoffmann *et al.*, Phys. Rev. Lett. **97**, 078301 (2006)
[9] F. Ebert *et al.*, Eur. Phys. J. E **26**, 161 (2008).
[10] L. Assoud *et al.*, Europhys. Lett. **80**, 48 001 (2007).
[11] H. Shintani and H. Tanaka, Nature Phys. **2**, 200 (2006).
[12] J.-P. Hansen and I. R. MacDonald, *Theory of Simple Liquids* (Academic, New York, 1986), 2nd ed.
[13] For a molecular glass former such as orthoterphenyl, the time for a fast quench is about 10^9 slower than a typical molecular motion.
[14] For an equilibrium molecular dynamics simulation for a similar model, see T. Stirner and J. Sun, Langmuir **21**, 6636 (2005).
[15] The selection criteria used here are more sensitive to the underlying crystal structure than the ordinary Voronoi tessellation; see J.-P. Eckmann and I. Procaccia, Phys. Rev. E **78**, 011503 (2008).
[16] The overshooting disappears for slower quenching.
[17] M. Bayer *et al.*, Phys. Rev. E **76**, 011508 (2007).
[18] T. Hamanaka and A. Onuki, Phys. Rev. E **75**, 041503 (2007).
[19] A. Widmer-Cooper and P. Harrowell, Phys. Rev. Lett. **96**, 185701 (2006).
[20] T. Kawasaki *et al.*, Phys. Rev. Lett. **99**, 215701 (2007).
[21] A. Libal *et al.*, Phys. Rev. E **75**, 011403 (2007).
[22] A. Pertsinidis and X. S. Ling, Nature (London) **413**, 147 (2001).
[23] A. Pertsinidis and X. S. Ling, Phys. Rev. Lett. **87**, 098303 (2001).